One-Dimensional Contact Mode Interdigitated Center of Pressure Sensor (CMIPS)

Tian-Bing Xu[1], Nelson Guerreiro[1,2], James Hubbard[1,2], Jin Ho Kang[1], Cheol Park[1,4], and Joycelyn Harrison[3]

1. National Institute of Aerospace, 100 Exploration Way, Hampton, VA 23666
2. University of Maryland, 3181 Martin Hall, College Park, MD 20742
3. NASA Langley Research Center, 6A West Taylor Street, Hampton, VA 23681
4. Department of Mechanical and Aerospace Engineering, University of Virginia, Charlottesville, VA 22904

A one dimensional contact mode interdigitated center of pressure sensor (CMIPS) has been developed. The experimental study demonstrated that the CMIPS has the capability to measure the overall pressure as well as the center of pressure in one dimension, simultaneously. A theoretical model for the CMIPS is established here based on the equivalent circuit of the configuration of the CMIPS as well as the material properties of the sensor. The experimental results match well with theoretical modeling predictions. A system mapped with two or more pieces of the CMIPS can be used to obtain information from the pressure distribution in multi-dimensions.

The measurement of pressure (force) distributions, *i.e.*, pressure maps, is an issue of importance in many fields such as biomedical research, chemical industry, and aerodynamic control.[1-3] For example, the measurement of real-time aerodynamic forces acting on an aircraft in flight is a challenging task. Typically, numerous arrays of pressure ports and transducers are built into the aerodynamic surfaces of the aircraft to provide a large number of discrete measurements of pressures at selected locations. Such a system is both mechanically complex and computationally intensive. Alternatively, several spatially-distributed sensor configurations have been developed.[4,5] The goal of the research presented herein is to design and test a simple sensor system that can be readily used for in-flight measurement of useful aerodynamic forces. In addition, these inexpensive pressure mapping sensors can also be used broadly, such as in smart car seats, intelligent sofas and beds, and smart shoes.[4,7,8] In this paper, a contact mode[1,6] interdigitated pressure sensor (CMIPS), which can measure the integrated pressure as well as center of pressure, simultaneously, is presented with modeling and experimentally validated results.

The linearly-weighted, spatially-distributed sensor configuration of the CMIPS used for this study is shown in Fig. 1. Figs. 1(a) and (b) are the cross section views in the length and width directions of the CMIPS, respectively. The CMIPS sensor is a three-layer design: the bottom layer is composed of a polyester film substrate with a screen-printed silver or silver/graphite interdigitated electrode as shown in Fig. 1(c), the middle layer is a 3M double-sided adhesive tape border that serves as a spacer between the top and bottom layers. The top sensor layer is composed of another polyester film substrate coated with a resistive ink print (RIP), which is a manufacturer's proprietary thin film

mixture, on its bottom side. When pressure/force is applied at a certain location, the top layer RIP makes contact with the bottom interdigitated electrode. The contact resistance depends on the surface properties of the electrode and the RIP, geometry of the electrode, and the applied pressure/force. For a specific CMIPS with pre-defined surface properties and electrode geometry, the contact resistance depends on the applied pressure/force only.

The diagram of the interdigitated electrode pattern investigated here is shown in Fig. 1(c). The sensor electrode aperture is patterned and applied to a rectangular piece of insulator film (polyester) with a metal conductive electrode on one side of the film. The metal electrode pattern is comprised of three groups (*A*, *B*, *C*) of metal lines. The group line *C* is a common interdigitated line group electrode and the main line spans the entire rectangular sensor aperture diagonally. The lines of group *A* form a triangular-shaped interdigitated group electrode, with resistance R_A, with the lines of the common group *C*. The lines of group *B* form the second triangular-shaped interdigitated electrode group, having resistance R_B, with the lines of the common group *C*. Each triangular group is an interdigitated pattern formed with N_0 pairs of parallel metal electrode lines. The overlap length of each of the N_i-pair of electrodes can be defined by a finite arithmetic sequence.

When the RIP comes in contact with the interdigitated electrode pattern, two types of resistances are produced. One type is contact resistance between the metal electrodes and the RIP. These changes in contact resistance constitute the pressure sensing mechanism, i.e., the contact resistance will rely on the contact area and the applied pressure. The other type of resistance is due to the conductivity of the RIP. For group resistance R_A, each interdigitated electrode line (i) of group *A* forms two film

resistances (R_{ACi1} and R_{ACi2}) with its two neighboring electrode lines from the common group *C*. There are also two contact resistances (R_{Ai1} and R_{Ci1}) from resistance R_{ACi1} to *A* and *C* terminals and another two contact resistances (R_{Ai2} and R_{Ci2}) from resistance R_{ACi2} to *A* and *C* terminals. The same geometry exists for group resistance R_B. The equivalent circuit of a CMIPS is shown in Fig. 2.

The two film resistances (R_{ACi1} and R_{ACi2}) in group resistance *A* can be expressed as[7]

$$R_{ACi1} = R_{ACi2} = (\rho_0 L_0)/(W_i t) = \rho_0 d_s /(i\Delta t_r), \qquad (1)$$

where ρ_0 is the resistivity of the RIP, t (= t_r) is the thickness of the RIP, L_0 (= d_s) is the length of the film resistance element, and W_i (= $i\Delta$) is the effective width of the film resistance, which is equal to the length of the overlap part of the finger electrode line.

Each contact resistance will be

$$R_x = \rho_{cp} /(w l_x) \qquad (2)$$

where w is the width of the electrode line; ρ_{cp} is the contact resistivity between the metal electrode and the RIP, which is pressure dependent; and x represents *Ai1*, *Ai2*, *Ci1*, and *Ci2*, and l_x is the length of the electrode line.

The resistance R_{Ai}, which originates from the terminal *A* through the electrode line A_i to the terminal *C*, is

$$R_{Ai} = \frac{(R_{Ci1} + R_{Ai1} + R_{ACi1})(R_{Ci2} + R_{Ai2} + R_{ACi2})}{R_{Ci1} + R_{Ai1} + R_{ACi1} + R_{Ci2} + R_{Ai2} + R_{ACi2}}. \qquad (3)$$

The total group resistance R_A, which is the total resistance from the terminal *A* to terminal *C*, is then

$$\frac{1}{R_A} = \sum_{i=1}^{N_0} \frac{1}{R_{Ai}}. \qquad (4)$$

Applying a similar treatment for the resistance R_B of group resistance B, the performance of the CMIPS was modeled based on the equivalent circuit in Fig. 2.

The CMIPS components were fabricated by Sensitronics, LLC, a sensor manufacturer. The sensor was assembled by first attaching the spacer layer to the bottom layer and then attaching the top layer to the spacer layer. Fig. 1(a) shows the lay-up configuration of the sensor. This configuration provides an open-circuit sensor when no load is being applied. The dimensions of the various parameters of the CMIPS tested are listed in the Table 1.

The sheet resistance of the RIP, which was 193,000 Ω/square, was measured using a Signatone S-301-4 four probe measurement station. The characterization of the CMIPS was done by applying a uniformly distributed load across the sensor width at specified length locations, as shown in Fig. 1(d). A 0.91 gram plastic beam with a dimension of 22 (length, which covers the width of the interdigitated electrode) × 5.65 (width, which covers three pairs of interdigitated lines) × 6.61(height) mm^3 served as the standing weight bar, and additional mass was applied to play the role of the applied force, covering three pairs of interdigitated lines, simultaneously. The resistances of R_A and R_B were measured with two Fluke 8842A multimeters. The contact resistivity ρ_{cp} between the metal electrode and the RIP for the sensor as a function of applied pressure was measured and is presented in Fig 3. The contact resistance decreased linearly with increasing applied force/pressure in log-log plot at the investigated pressure range.

The conductance G (inverse of resistance) versus location for R_A and R_B of the CMIPS at different pressures was measured and is shown in Fig. 4. The lines are theoretically predicted results and the symbols are experimentally measured data. The

experimental results agreed well with the predicted results for most cases. When an applied constant mechanical load (equivalent to pressure), as shown in Fig. 1(d), moved along the sensor aperture length from left to right, the conductance G_A (= $1/R_A$) of group resistance R_A increased linearly while the conductance G_B (=$1/R_B$) of group resistance R_B decreased linearly. The ratio of G_A to the sum of G_A and G_B is related to the normalized location of the center of pressure while the sum of G_A and G_B itself is related to the integrated pressure on the sensor.

Furthermore, the resistance ratio of $R_A/(R_A+R_B)$ is almost linearly dependent on the location of the center of force, as shown in Fig. 5. The slopes of the lines listed in Table 2 for the resistance ratios versus location decreased less than 5% when the pressure increased 10 times, and the experimental data agreed with theoretical predictions. Both theoretical prediction and experimental validation indicate that the center location of the pressure can be identified by the resistance ratio of $R_A/(R_A+R_B)$, and the total applied pressure on the sensor can be determined by the sum of the resistances of groups R_A and R_B. Therefore, the CMIPS with the electrode spatial weighting used in this study enables the measurements of the overall pressure and the location of the pressure center, simultaneously.

In summary, a contact mode interdigitated pressure sensor (CMIPS) was developed. Both theoretical prediction and experimental validation demonstrated that the CMIPS has the capability to measure overall pressure as well as the center of pressure, simultaneously. A theoretical model for the CMIPS was established based on the configurations of the sensor as well as the material properties of the sensor. The experimental data agree well with the theoretically predicted results. Although the

CMIPS can only integrate the pressure distribution in one dimension, the information from pressure distributions in three dimensions can be provided by mapping two or more pieces of the CMIPS.

The authors thank Mr. James High and Mrs. Nancy Holloway at NASA Langley Research Center for their technical support and Franklin Eventoff of Sensitronics, LLC for manufacturing the sensor.

Figure Captions:

Fig. 1. Diagram of the CMIPS. (a) is the cross section view in the length direction, (b) is the cross section view in the width direction, (c) is the patterned interdigitated bottom electrode on a plastic substrate, and (d) is the cross section view in the width direction when a pressure or force is applied during measurement.

Fig. 2 Equivalent circuit of the CMIPS.

Fig. 3. The contact resistivity between the metal electrode and the surface of the RIP as a function of applied pressure.

Fig. 4. The conductance vs. location for groups A and B of the CMIPS at different pressures. The lines (black solid for G_A and green dash for G_B) from bottom to top are theoretical modeled results for pressure at 2.29, 5.72, 11.44, and 22.89 psi, respectively. The symbols are experimental results for applied pressure at 2.29 (■ for G_A and □ for G_B), 5.72 (● for G_A and ○ for G_B), 11.44 (▲ for G_A and △ for G_B), and 22.89 (▼ for G_A and ▽ for G_B) psi, respectively. The measurement error bars are also presented.

Fig. 5. The ratio of $R_A/(R_A+R_B)$ vs. location for the CMIPS at different pressures. The four solid lines are theoretically predicted results for pressure at 2.29, 5.72, 11.44, and 22.89 psi, respectively. The symbols are experimental results for applied pressure at 2.29 (▽), 5.72 (△), 11.44 (○), and 22.89 (□) psi, respectively.

References

1. Z. Del Prete, L. Monteleone, and R. Steindle, Rev. Sci. Instrum. **72**, 1548 (2001).
2. D. Keats-Pullen, J. E. Hubbard, Jr., and N. Guerreiro, J. Intel. Mater. Sys. Struct. **19**, 837 (2008).
3. L. Mohanty and S. C. Tjin, Appl. Phys. Lett. **88**, 083901 (2006).
4. J. E. Hubbard, Jr., U.S. Patents No. **5,821,633** (1998), No. **5,797,623** (1998), **6,223,606** (2001), No. **6,223,606 B1** (2001), **6,360,597 B1** (2002), and **6,546,813 B2** (2003).
5. J. E. Hubbard, Jr. and D. Keats-Pullen, U.S. Patent No. **7,415,876 B2** (2008).
6. T. V. Papakostas, J. Lima, and M. Lowe, Sensors Proceeding of IEEE **2**, 1620 (2002).
7. M. Fogiel, The Handbook of Electrical Engineering, Research & Education Association, Piscataway, NJ (1996).
8. L. Barna, M. Koivuloma, M. Hasu, J. Tuppurainen, and A. Varri, IEEE Sensors J. **7,** 74 (2007).

Table 1. List of the CMIPS sensor parameters and dimensions.

Parameters	Symbol	Numbers	Dimension Value (mm)
Width of electrode finger	d_e		0.381
Spacing of electrode finger	d_s		0.381
Number of electrode fingers	n_f	319	
Number of electrode finger pairs	N_0	159	
Lengths of the shortest electrode finger of R_A and R_B	l_0		1.016
Lengths of the longest electrode finger of R_A and R_B	l_{N0}		22.987
Length increment of next electrode finger of R_A and R_B	Δ		0.139
Length of electrode (active)	L_e		242.7
Length of sensor substrate	L_s		244.5
Thickness of the air gap	t_{ag}		0.078
Thickness of the electrode	t_{ie}		0.002
Thickness of the lower substrate	t_{ls}		0.175
Thickness of RIP	t_r		0.010
Thickness of the spacer	t_{sp}		0.090
Thickness of the upper substrate	t_{us}		0.125
Width of the electrode (active)	W_e		25.4
Width of the sensor substrate	W_s		28.58

Table 2. List the slopes of the resistance ratio of $R_A/(R_A+R_B)$ versus locations for CMIPS sensor at different applied pressures.

Pressure (psi)	2.29	5.72	11.44	22.89
Slope (1/mm)	-0.00372	-0.00377	-0.00383	-0.00388

Fig. 1 Xu, et al.

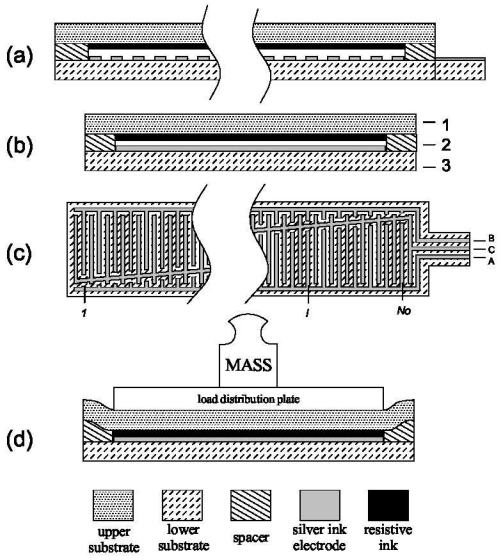
(a)
(b)
1
2
3
(c)
B
C
A
1
i
No
MASS
load distribution plate
(d)
upper substrate
lower substrate
spacer
silver ink electrode
resistive ink

Fig. 2 Xu, et al.

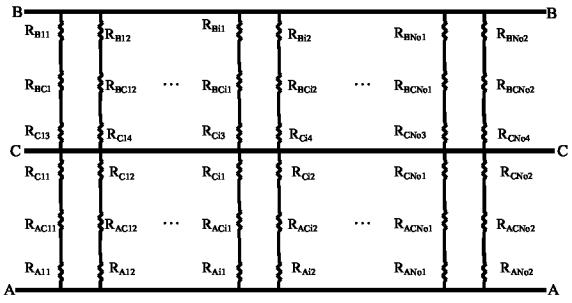
B
B
C
C
A
A
R_{B11}
R_{B12}
R_{Bi1}
R_{Bi2}
R_{BNo1}
R_{BNo2}
R_{BC1}
R_{BC12}
R_{BCi1}
R_{BCi2}
R_{BCNo1}
R_{BCNo2}
R_{C13}
R_{C14}
R_{Ci3}
R_{Ci4}
R_{CNo3}
R_{CNo4}
R_{C11}
R_{C12}
R_{Ci1}
R_{Ci2}
R_{CNo1}
R_{CNo2}
R_{AC11}
R_{AC12}
R_{ACi1}
R_{ACi2}
R_{ACNo1}
R_{ACNo2}
R_{A11}
R_{A12}
R_{Ai1}
R_{Ai2}
R_{ANo1}
R_{ANo2}

Fig. 3 Xu, et al.

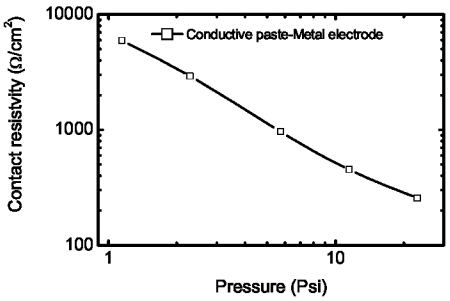
Conductive paste-Metal electrode
Contact resistivity (Ω/cm²)
10000
1000
100
1
10
Pressure (Psi)

Fig. 4 Xu, et al.

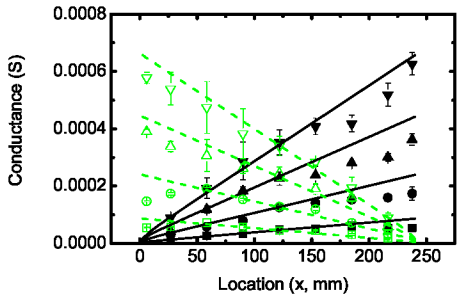
0.0008
0.0006
0.0004
0.0002
0.0000
Conductance (S)
0
50
100
150
200
250
Location (x, mm)
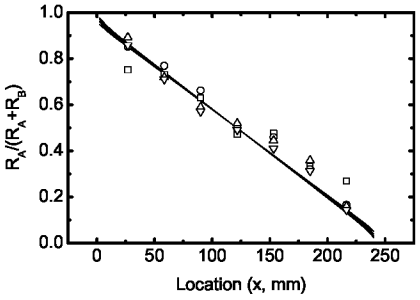
Fig. 5 Xu, et al.